

7-5-79

INTERIM REPORT
NRC Research and Technical
Assistance Report

Accession No. _____

Contract Program or Project Title:

Subject of this Document: "Cladding Mechanical Limits (CMLIMT)"

Type of Document:

Author(s): D. L. Hagrman

Date of Document: May 1979

Responsible NRC Individual and NRC Office or Division: G. Marino

This document was prepared primarily for preliminary or internal use. It has not received full review and approval. Since there may be substantive changes, this document should not be considered final.

Kay Rose

for
H. P. Pearson, Supervisor
Information Processing
EG&G Idaho

Prepared for
U.S. Nuclear Regulatory Commission
Washington, D.C. 20555

NRC Fin #A6046

INTERIM REPORT

NRC Research and Technical
Assistance Report

7908010 458

51A 247

CDAP-TR-056

for U.S. Nuclear Regulatory Commission

**CODE DEVELOPMENT AND ANALYSIS PROGRAM
CLADDING MECHANICAL LIMITS
(CMLIMT)**

D.L. HAGRMAN

May 1979



EG&G Idaho, Inc.



IDAHO NATIONAL ENGINEERING LABORATORY

DEPARTMENT OF ENERGY

IDAHO OPERATIONS OFFICE UNDER CONTRACT EY-76-C-07-1570

514 248

NOTICE

This report was prepared as an account of work sponsored by the United States Government. Neither the United States nor the Department of Energy, nor the Nuclear Regulatory Commission, nor any of their employees, nor any of their contractors, subcontractors, or their employees, makes any warranty, express or implied, or assumes any legal liability or responsibility for the accuracy, completeness or usefulness of any information, apparatus, product or process disclosed, or represents that its use would not infringe privately owned rights.

CONTENTS

FOREWORD.	i
11. CLADDING MECHANICAL LIMITS (CMLIMT).	1
11.1 Summary.	1
11.2 Available Data	4
11.3 Model Development.	11
11.4 Application of the Failure Criterion to Determine Cladding Shape after Burst	23
11.5 Cladding Mechanical Limits Subcode CMLIMT Listing.	34
11.6 References	40

LIST OF FIGURES

B-11.1	Local radial strains at burst versus temperature.	15
B-11.2	Average circumferential strains at failure versus temperature.	16
B-11.3	Local tangential stress at failure versus temperature . . .	19
B-11.4	Base data and MATPRO correlation for effect of temper- ature variation on average circumferential elongation . . .	27
B-11.5	Schematic cross sections of cladding at burst	29
B-11.6	Typical average circumferential strains predicted by the MATPRO correlations for typical engineering burst stress, true burst stress and typical cir- cumferential strain distribution.	35

LIST OF TABLES

B-11.I	Summary of Multirod Burst Test Data Employed in CMLIMT	6
B-11.II	Summary of Data from the Hobson-Rittenhouse Tests	7
B-11.III	Summary of Data from the Chung-Kassner Tests.	8
B-11.IV	Summary of Data from the Bauer et al Tests.	10
B-11.V	Listing of the CMLIMT Code.	36

FORWARD

This report describes revised models for cladding mechanical limits. It will become part of an update to the Materials Properties (MATPRO) Handbook^a used in the fuel rod behavior modeling task performed at EG&G Idaho, Inc.

The update incorporates important new data from several Nuclear Regulatory Commission and German experimental programs and defines a single physically reasonable failure criterion for cladding under tensile stress. Alternate simplified expressions are also derived for use in obtaining estimates of typical cladding shape after burst.

Many of the data were obtained from photographs of cladding cross sections sent to the author by experimenters. The author would like to thank R. H. Chapman and D. O. Hobson of the Oak Ridge National Laboratory, A. A. Bauer and L. W. Lowry of Battelle Columbus Laboratories and H. M. Chung and T. F. Kassner of the Argonne National Laboratory for providing these photographs. He would also like to thank S. Dagbjartsson, F. Erbacher, E. Karb and K. Wiehr for providing data from Germany and for several enlightening discussions of these data.

a D. L. Hagerman and G. A. Reymann (Eds), MATPRO Version 11 - A Handbook of Materials Properties for use in the Analysis of Light Water Reactor Fuel Rod Behavior, TREE-1280, NUREG-CR-0497, (February 1979).

The format and numbering scheme used in this report are consistent with its intended use in an update of the MATPRO handbook. It is beyond the scope of this report to provide a complete description of the MATPRO package and its organization. Readers who require descriptions of the use materials properties subcodes should consult the code descriptions^{a,b}.

-
- a G. A. Berna et al, FRAPCON-1: A Code for the Steady-State Analysis of Oxide Fuel Rods, CDAP-TR-78-032-R1, (November 1978).
- b L. J. Siefken et al, FRAP-T5: A Computer Code for Transient Analysis of Oxide Fuel Rods - Volume I - Analytical Models and Input Manual, CDAP-TR-79-43, (March 1979).

11. CLADDING MECHANICAL LIMITS (CMLIMT)

(D. L. Hagrman)

Cladding mechanical limits are important to code predictions of both the number of failed rods and the shape of those rods that have failed. This section describes expressions used to determine the most important limits, the elastic-plastic transition (yield) and cladding failure under tensile stress, as well as the ultimate engineering strength and the uniform elongation.

The form of the expressions used to describe mechanical limits is related to the particular stress-strain relation assumed in the MATPRO package. Expressions for failure are also related to the amount of detail the user chooses to consider in mechanical models. The fundamental failure criterion is derived for codes that model cladding plastic deformation without assuming azimuthally symmetric deformation. Alternate expressions are presented for less sophisticated codes which do assume symmetric deformation. Also, one simplified correlation is presented for users who do not model plastic deformation at all.

11.1 Summary

The CMLIMT subcode uses input values of temperature, cold work, fast neutron fluence ($E > 1$ MeV), average oxygen concentration and strain rate to define a yield point and the maximum load for one dimensional stress. The equations used are:

$$\text{True Strain at Yield} = \left[\frac{K}{E} \left(\frac{\dot{\epsilon}}{10^{-3}} \right)^m \right]^{\frac{1}{1-n}} \quad (\text{B-11.1})$$

$$\text{True Yield Strength} = \left[\frac{K}{E^n} \left(\frac{\dot{\epsilon}}{10^{-3}} \right)^m \right]^{\frac{1}{1-n}} \quad (\text{B-11.2})$$

$$\text{True Strain at Maximum Load} = \frac{n}{1+n} \quad (\text{B-11.3})$$

$$\text{True Ultimate Strength} = K \left(\frac{\dot{\epsilon}}{10^{-3}} \right)^m \left(\frac{n}{1+n} \right) \quad (\text{B-11.4})$$

where

- K = strength coefficient (Pa)
- n = strain hardening exponent (unitless)
- $\dot{\epsilon}$ = true strain rate (s^{-1})
- m = strain rate sensitivity constant (unitless)
- E = Young's modulus (Pa).

K, n and m are calculated with the subcode CKMN discussed in the description of CSTRES (Section B-8, this appendix)^a, E is obtained by calling the function CELMOD (Section B-5, this appendix), and $\dot{\epsilon}$ is required input information.

Arguments are presented in Section 11.3 which demonstrate that cladding failure should be predicted by comparing the tangential component of true stress to the burst stress. Heating rate and strain rate do not affect this criterion but irradiation and cold work increase it somewhat. The burst stress as a function of temperature is given by the following expressions.

a The version of the CSTRES subcode which will be used in the MATPRO-12 handbook was published as interium report CDAP-TR-78-048.

For temperatures less than or equal to 750 Kelvin,

$$\sigma_{\theta B} = 1.36 K_A \quad (B-11.5a)$$

For temperatures between 750 and 1050 Kelvin,

$$\sigma_{\theta B} = 46.861429 K_A \exp \left(- \frac{1.9901087 \cdot 10^6}{T^2} \right) \quad (B-11.5b)$$

For temperatures greater than 1050 Kelvin,

$$\sigma_{\theta B} = 7.7 K_A \quad (B-11.5c)$$

where

$\sigma_{\theta B}$ = tangential component of true stress at burst (Pa)

K_A = strength coefficient for annealed cladding as determined with the MATPRO-12 CKMN subcode (Pa)

T = temperature (degrees Kelvin).

For cold worked or irradiated cladding the burst stress is increased by four tenths of the increase of the strength coefficient due to irradiation and cold work.

The standard error^a of Equations (B-11.5) is found to be

$$U\sigma_{\theta B} = 0.17\sigma_{\theta B} \quad (B-11.6)$$

a The standard error of a model is estimated with a set of data by the expression: (sum of squared residuals/number of residuals minus the number of constants used to fit the data)^{1/2}.

Section 11.2 is a review of the available data. Equations (B-11.1) through (B-11.6) are derived in Section 11.3 and alternate methods of applying Equation (B-11.5) are derived in Section 11.4. Section 11.5 is a listing of the subcode CMLIMT and references are contained in Section 11.6.

11.2 Available Data

The data reported as yield points, strain at maximum load (uniform strain) and ultimate strength have been reviewed in conjunction with the description of the CSTRÉS code (Section B-8 of this appendix). This subsection will review only the data used in the development of the CMLIMT subcode failure criterion. The number of these data has been severely restricted by the requirement that they be sufficiently complete to allow an estimate of local stresses and strain at failure.

The most useful data have been produced by the Multirod Burst Test Program conducted by the U.S. Nuclear Regulatory Commission. All of these data were obtained with internal heaters and an external steam environment. Heating rates varied from 0 to 28 K/s. Estimated burst temperatures, burst pressures and burst strains (average circumferential elongation) have been published for a number of single rod tests^{B-11.1, B-11.2}. In addition, calibrated photographs of cross sections through the burst regions of some of the tests have been published^{B-11.2, B-11.3, B-11.4, B-11.5}. These cross sections were needed to estimate wall thickness at burst^a for the calculation of local stress at failure. The other required information for the local stress analysis which will be developed in Section 11.3 is an estimate of the axial radius of curvature at burst. This information was not published but could be estimated with sufficient accuracy from side

a Most burst edges displayed one or more cleavage-like lines approximately 45 degrees from the radial direction. The wall thickness was measured adjacent to this line or, if the line could not be distinguished, 0.25 mm from the burst tear.

view photographs of the burst tubes^{B-11.6, B-11.7, B-11.8}. Table B-11.1 is a summary of the Multirod Burst Test Program data that were used.

Data from tests by Hobson and Rittenhouse^{B-11.9} were also employed. The Hobson-Rittenhouse tests were conducted with a radiant heating furnace on BWR cladding in an argon environment with heating rates from 5.6 to 56 K/s. During the early stages of the analysis these data were treated with considerable suspicion because they do not include the effects of a steam environment. However, as the analysis progressed it became clear that there was no significant difference in the local failure stress predicted from the Hobson-Rittenhouse data and the local failure stress predicted from the available tests in a steam environment. It is possible that long-time tests in steam will show a significant difference in local stress at failure when they become available. However, it is also possible that tests which oxidize for relatively long times before significant deformation occurs will show that the oxygen rich layers of the cladding rupture before the oxygen-poor layers rupture. In the latter case oxidation would have a significant effect on the early (small strain) deformation but little effect on the stress at failure.

Table B-11.II is a summary of the data from the tests by Hobson and Rittenhouse that were used. Burst temperatures, wall thickness measurements and the average circumferential elongation were obtained from figures in Reference B-11.9. Burst pressures were obtained by private communication from R. H. Chapman and axial radii of curvature were estimated from samples sent by D. O. Hobson.

Table B-11.III is a summary of data obtained by H. M. Chung and T. F. Kassner^{B-11.10} which were used in the development of the CMLIMT code. The burst temperature, differential pressure at burst, average circumferential strain and axial radius of curvature were obtained from Reference B-11.10. The wall thickness at burst was obtained from

TABLE B-11.1

SUMMARY OF MULTIROD BURST TEST DATA EMPLOYED IN CMLIMT

Test No.	Burst Temperature (K)	Differential Pressure at Burst (MPa)	Average Circumferential Strain (m/m)	Wall Thickness at Burst (mm)	Axial Radius of Curvature (cm)
PS-10	1174 ^a	6.000 ^a	0.20 ^a	0.079 ^c	2.1 ^c
PS-17	1051 ^a	12.130 ^a	0.25 ^a	0.176 ^c	1.2 ^c
PS-18	1444 ^a	0.772 ^a	0.24 ^a	0.111 ^d	0.9 ^g
PS-19	1232 ^a	2.590 ^a	0.28 ^a	0.079 ^c	0.6 ^c
SR-23	1350 ^a	0.960 ^a	0.35 ^a	0.164 ^e	1.1 ^h
SR-25	1365 ^a	0.960 ^a	0.78 ^a	0.077 ^e	0.6 ⁱ
SR-34	1039 ^b	5.820 ^b	0.316 ^b	0.109 ^b	1.6 ^c
SR-35	1048 ^b	4.470 ^b	0.290 ^b	0.073 ^f	3.1 ^c
SR-37	1023 ^b	13.560 ^b	0.231 ^b	0.263 ^f	3.7 ^c
SR-41	1030 ^b	9.765 ^b	0.274 ^b	0.199 ^b	2.7 ^c
SR-43	1046 ^b	7.620 ^b	0.200 ^b	0.179 ^b	3.5 ^c

- a Reference B-11.1, pages 18 and 19
 b Reference B-11.2, pages 7 and 31
 c From photographs sent by R. H. Chapman
 d Reference B-11.3, page 35
 e Reference B-11.4, pages 120, 121
 f Reference B-11.5, page 26
 g Reference B-11.6, page 19
 h Reference B-11.7, page 22
 i Reference B-11.8, page 17

TABLE B-11.11

SUMMARY OF DATA FROM THE HOBSON-RITTENHOUSE TESTS

Test No.	Burst Temperature (K)	Differential Pressure at Burst (MPa)	Average Circumferential Strain (m/m)	Wall Thickness at Burst (mm)	Axial Radius of Curvature (cm)
35	1061	6.170	0.63	0.25	2.9
34	1081	7.584	0.58	0.23	1.8
40	1111	4.654	0.79	0.18	1.8
18	1145	4.826	1.25	0.18	3.0
17	1158	4.205	0.57	0.20	2.5
19	1160	4.895	0.51	0.23	1.8
21	1171	3.102	0.30	0.18	1.7
8	1179	3.826	0.22	0.20	1.3
16	1195	3.999	0.42	0.25	1.7
5	1196	3.757	0.44	0.20	1.0
26a	1205	3.068	0.27	0.28	1.8
27	1213	2.241	0.55	0.15	1.1
15	1214	2.275	0.41	0.18	1.1
37	1215	2.344	0.40	0.18	1.4
26	1220	3.033	0.53	0.13	1.5
9	1235	1.448	0.43	0.20	2.7
28	1253	1.413	0.85	0.18	2.3
11	1299	1.434	0.68	0.25	1.5
32	1302	0.745	0.93	0.25	2.1
29	1432	0.676	0.92	0.23	2.5
36	1440	0.827	0.50	0.23	1.5
4	1472	0.689	1.11	0.20	2.5
36a	1487	0.662	0.74	0.25	1.5

TABLE B-11.III

SUMMARY OF DATA FROM THE CHUNG-KASSNER TESTS

<u>Test No.</u>	<u>Burst Temperature (K)</u>	<u>Differential Pressure at Burst (MPa)</u>	<u>Average Circumferential Strain (m/m)</u>	<u>Wall Thickness at Burst (mm)</u>	<u>Axial Radius of Curvature (cm)</u>
AS-40	1089	5.352	1.01	0.39	2.9
AS-36	1310	0.558	1.11	0.26	2.9
AS-9	1329	1.282	1.24	0.12	3.2
AS-5	1348	1.334	1.02	0.42	1.6

photographs of cross sections obtained from Chung by private communication. It is important to note that all of the tests in Table B-11.III were constrained by an internal mandrel which applied an unknown axial stress to the cladding.

None of the data mentioned so far were obtained from irradiated cladding or at temperatures below 1000 K. The only available low temperature data with irradiated cladding were obtained from studies by A. A. Bauer, L. M. Lowry, W. J. Gallagher, A. J. Markworth and J. S. Perrin^{B-11.11, B-11.12, B-11.13} on cladding obtained from the H. B. Robinson reactor. The data from Bauer et al which were used in the development of CMLIMT are presented in Table B-11.IV. Tests M12-16, M12-4 and M12-15 were conducted on as received cladding while tests D9-7, D9-8, D9-13 and D9-14 were conducted on cladding which had been annealed. Wall thicknesses adjacent to the burst were obtained from unpublished photographs similar to Figure 7 of Reference B-11.11. The axial radii of curvature in these tests is unknown.

Two sources of in-reactor data were employed. One is the irradiation effects test IE-5 conducted in the Power Burst Facility at the Idaho National Engineering Laboratory^{B-11.14, B-11.15}. The measured internal pressure in this test was reported (page 12 of Reference B-11.15) to be 5.2 MPa in excess of the coolant pressure and the cladding temperature was estimated from microstructure studies to be near 1100 K. The average circumferential elongation was reported to be 25% (page 16 of Reference B-11.15). The wall thickness at burst was estimated from Figure 5 of the post examination results report to be 0.09 mm and the axial radius of curvature was estimated to be approximately four times the rod diameter from the posttest view on page 91 of Reference B-11.15.

The second source of in-reactor data is a series of tests in the FR2 reactor in Germany^{B-11.16}. Complete data from three tests were presented (A2.3, B1.2 and B1.3) but two of the cladding cross sections

TABLE B-11. IV

SUMMARY OF DATA FROM THE BAUER ET AL TESTS

Test No.	Burst Temperature ^a (K)	Burst Strength ^a (MPa)	Average Circumferential Strain ^a (m/m)	Wall Thickness at Burst ^b (mm)
M12-16	477	749.4	0.026	0.57
M12-4	644	659.1	0.052	0.60
M12-15	644	684.6	0.028	0.61
D9-7	644	356.4	2.212	0.46
D9-8	644	350.9	0.204	0.46
D9-13	644	372.3	0.225	0.51
D9-14	644	367.5	0.292	0.48

a From Reference B-11.12, pages 3 and 7

b From photographs sent by A. A. Bauer and L. W. Lowry

showed evidence of contact with the snroud (burst edges rolled in) and a possible change of the stress at burst. For that reason only data from test B1.2 were used. The average circumferential elongation, axial radius of curvature, burst pressure, and temperature for this test were taken from Figure 21 of Reference B-11.16 (0.249, 1.5 cm, 4.52 MPa, and 1188 K). The coolant pressure was assumed to be the typical value of 0.3MPa quoted on page 2.

One out-of-pile test result from Germany^{B-11.17} was used in developing the CMLIMT failure model. The test was performed in air (one atmosphere) with an internal heater. The burst temperature, internal pressure at burst, average circumferential strain and wall thickness at burst (1114K, 7.1MPa, 0.37, and 0.215mm) were taken from Figure 13 of Reference B-11.17. The axial radius of curvature was estimated to be approximately three times the cladding radius at burst by inspection of X-ray photos of similar tests just prior to burst.

11.3 Model Development

The expressions used to describe the elastic-plastic transition (Yield) do not correspond to the usual definition of Yield (stress at 0.2% strain). In order to provide expressions which are consistent with code requirements for continuous stress-strain expressions, the yield point is taken to be the nonzero intersection of the stress-strain curves given by Hooke's law for the elastic region

$$\sigma = E \epsilon \quad (B-11.7)$$

and by the modified power law used in CSTRES and CSTRAN for the plastic region

$$\sigma = K \epsilon^n \left(\frac{\epsilon}{10^{-3}} \right)^m \quad (B-11.8)$$

where

σ = true stress (Pa)

ϵ = true strain (unitless)

$\dot{\epsilon}$ = true strain rate (s^{-1})

E = Young's modulus (Pa)

K = strength coefficient (Pa)

n = strain hardening exponent (unitless)

m = strain rate sensitivity exponent (unitless).

Solution of these simultaneous equations gives the yield strain and yield strength described by Equations (B-11.1) and B-11.2), respectively.

The point of maximum load in a one dimensional stress test at constant engineering strain rate is found by converting the true stress and true strain rate in Equation (B-11.8) to their engineering equivalents

$$\sigma = S \exp (\epsilon) \quad (B-11.9)$$

$$\dot{\epsilon} = \dot{\epsilon} / \exp (\epsilon) \quad (B-11.10)$$

where

S = engineering stress (Pa)

$\dot{\epsilon}$ = engineering strain rate (s^{-1}).

The derivative of S with respect to ϵ is zero at the true strain given by Equation (B-11.3) and the true stress at this strain is given by Equation (B-11.4).

The development of Equation (B-11.5) was preceded by a review of the several different cladding failure criteria that have been in use. Two previously used criteria, average circumferential elongation and engineering hoop stress, were rejected because they ignore the effect of local wall thinning and because this effect is now realized to vary considerably from test to test^{B-11.4, B-11.10, B-11.16}. Two other possible criteria, strain rate at failure and strain-fraction rules (strain increment/strain at failure), were considered and rejected because these criteria would require a considerable collection of strain versus time data. Such a collection does not exist in the publicly-available literature. The remaining criteria, local strain at failure and local stress at failure, were investigated with the data presented in Section 11.2.

Local strain at failure was determined using the measured wall thickness adjacent to the burst^a

$$\epsilon_r = \ln \left(\frac{t_B}{t_0} \right) \quad (\text{B-11.11})$$

where

ϵ_r = true radial strain at burst

t_0 = initial cladding wall thickness

t_B = cladding wall thickness adjacent to burst

a Since the material is not compressible, the sum of the axial and circumferential strains is $-\epsilon_r$.

Figure B-11.1 is a plot of the local radial strains at burst versus temperature. Although considerable scatter is apparent from the plot it must be remembered that strain is a very sensitive parameter^a. The more relevant observations are:

- (a) The scatter of the local strains at failure is much smaller than the scatter of the average circumferential strains at failure for these tests. The average strains are shown in Figure B-11.2.
- (b) The series of tests by Chapman with decreasing pressures and heating rates but similar heaters, burst temperatures and average circumferential elongations -- SR-37, SR-41, SR-43, SR-34 and SR-35 -- show a regularly decreasing wall thickness (more negative radial strain) with decreasing pressure.

These observations suggest that the local stress is the common parameter of the cladding as it is about to burst. The data in the plot of local strains at failure versus temperature is scattered by neglected variations in circumferential radii of curvature, axial radii of curvature and burst pressure and the data in the plot of average circumferential strain at failure is scattered further by circumferential variations in strain. More evidence for using stress as the failure criterion is provided by the observations that (a) Failure cross sections usually show a fracture surface or surfaces at 45° to the tangential direction and in the direction of maximum shear stress; (b) The fracture line is usually longitudinal. In cases where the fracture line is circumferential, there is good reason to suspect large axial stress components (See Reference B-11.10, pages 86 and 87).

a The strain hardening exponent and the strain rate sensitivity exponent in Equation (B-11.8), are typically in the range 0.05-0.3. The small exponents mean small changes in stress will yield large changes in strain near failure because the stress versus strain and strain rate surface is flat. Thus, a lot of scatter in a strain versus temperature plot does not necessarily mean strain is a poor parameter for determining failure.

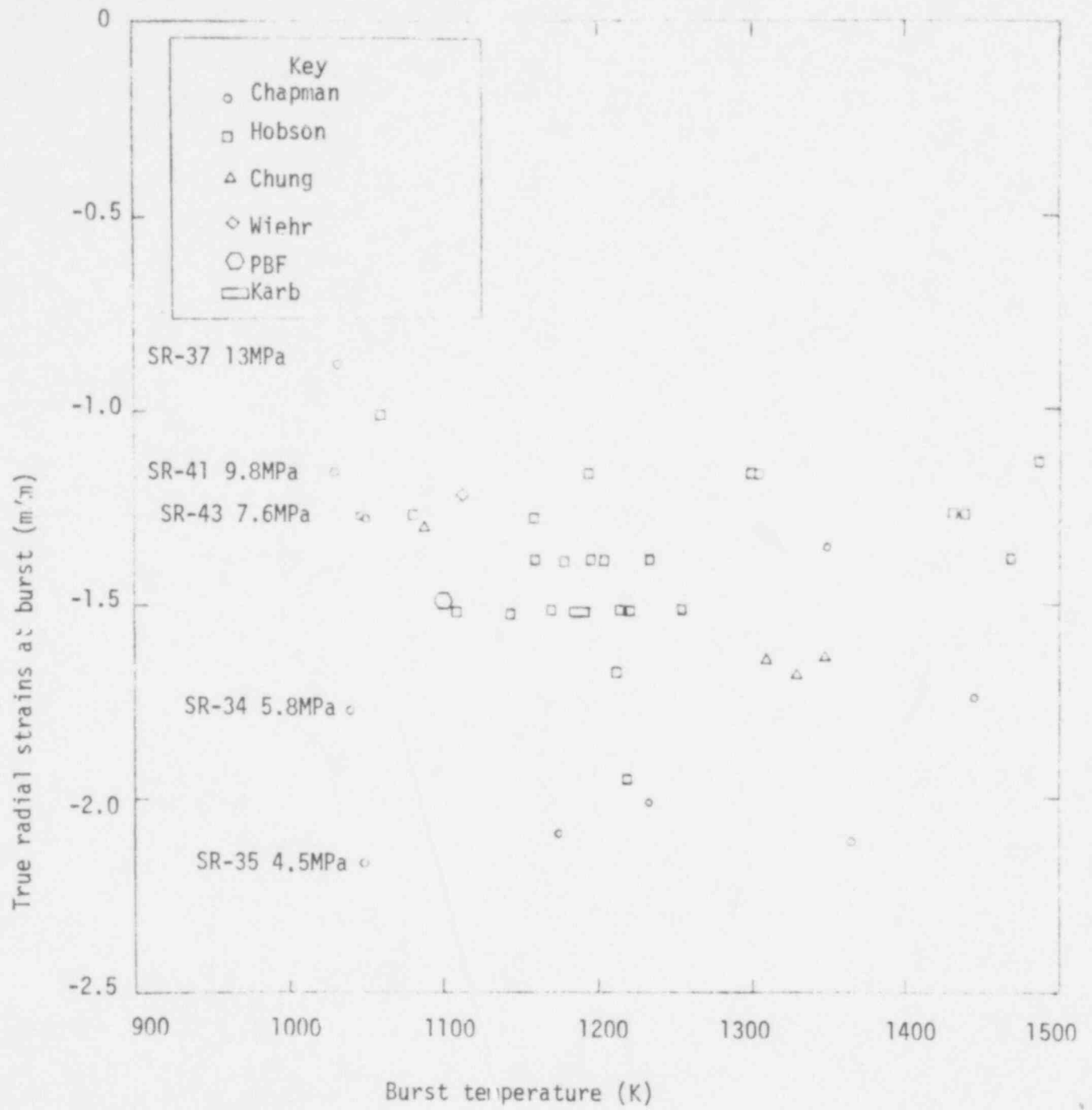


Fig. B-11.1 Local radial strains at burst versus temperature.

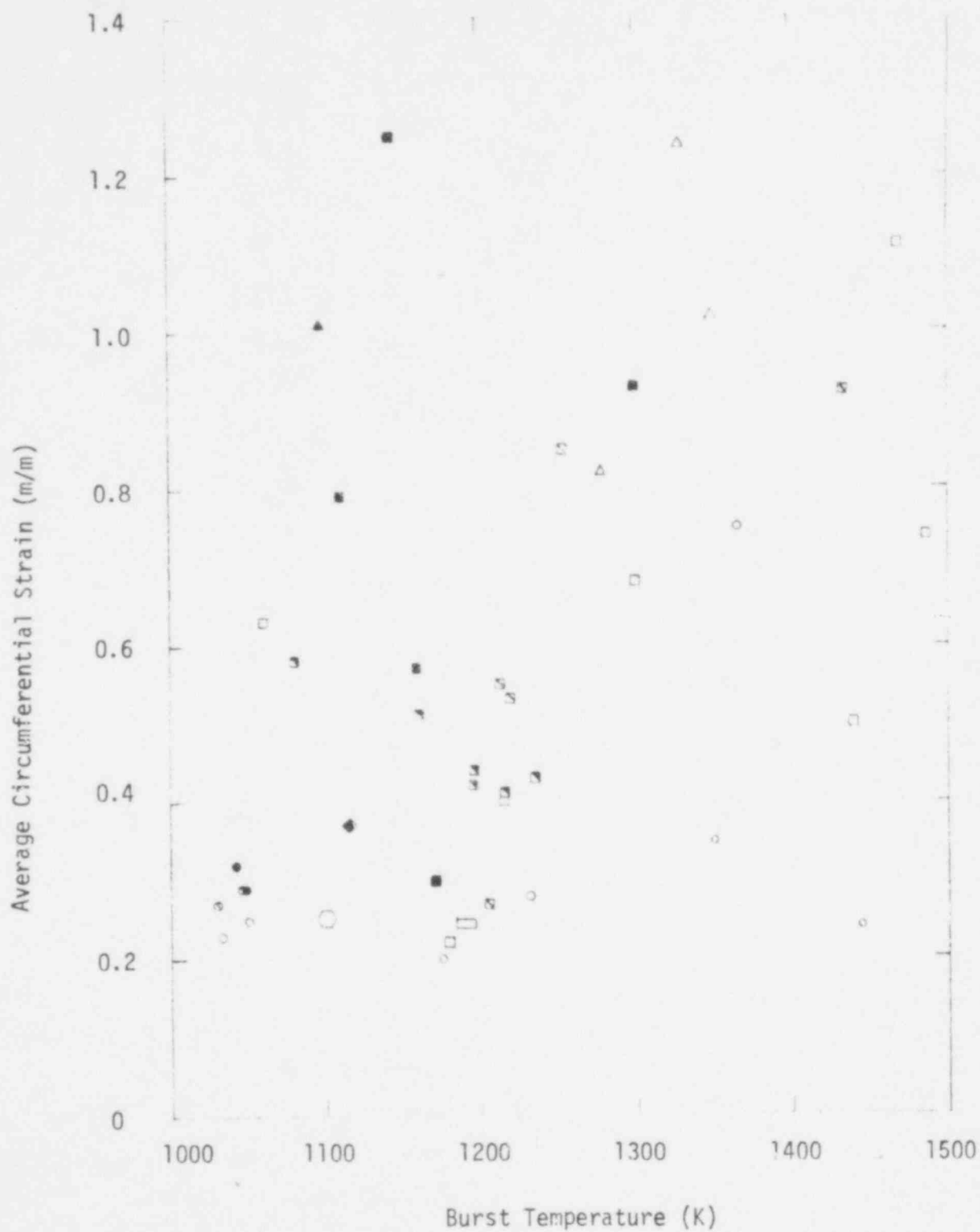


Fig. B-11.2 Average circumferential strains at failure versus temperature.

The observations mentioned above have led the author to conclude that local hoop stress is the best failure criterion for cladding burst. There are, however, two disadvantages associated with this approach. First, local true hoop stress is difficult for codes to calculate and, second, large changes in strain or strain rate are associated with small changes in stress. Neither disadvantage is insurmountable but some caution must be exercised in using the failure criterion that results from considering local true hoop stress. This point will be discussed further in Section 11.4.

Local stresses at failure were estimated from the data presented in Section 11.2 and the equilibrium equation for a membrane element at the moment of failure^{B-11.18}

$$\frac{\sigma_{ZB}}{r_Z} + \frac{\sigma_{\theta B}}{r_{\theta}} = \frac{P_B}{t_3} \quad (B-11.12)$$

where

P_B = difference between internal gas pressure and coolant pressure at burst

σ_{ZB} = axial stress at burst

$\sigma_{\theta B}$ = tangential stress at burst

r_Z = axial radius of curvature at burst

r_{θ} = circumferential radius of curvature at burst

t_3 = cladding thickness at burst.

Two approximations are needed to deduce $\sigma_{\theta B}$ from Equation (B-11.12) and the data that were presented in Section 11.2. The first approximation assumes the azimuthal cross section shortly before burst is approximately circular.

$$r_{\theta} \approx \text{undeformed radius} (1 + \text{average circumferential strain}) \quad (\text{B-11.13})$$

The second approximation is needed to estimate σ_{zB} . The range of possible values for σ_{zB} is rather severely limited by physical considerations. It must have been greater than the yield stress for significant ballooning to occur^{B-11.18} and it must have been less than $\sigma_{\theta B}$ for the failure to occur along an axial line. Since r_z is typically several times r_{θ} the first term of Equation (B-11.12) is small and any value of σ_{zB} in the range between the yield stress and $\sigma_{\theta B}$ will estimate the first term of the equation with uncertainty that is less than the uncertainty in the terms containing r_{θ} and t_B . The CMLIMT expression for failure stress was developed with the assumption that the axial and tangential stresses are nearly equal at burst because that assumption tends to underpredict $\sigma_{\theta B}$ while the assumption of Equation (B-11.13) tends to overpredict $\sigma_{\theta B}^a$. The resultant expression for the tangential stress at burst is

$$\sigma_{\theta B} \approx \frac{P_B}{t_B} \left[\frac{1}{\frac{1}{r_z} + \frac{1}{r_{\theta}}} \right] \quad (\text{B-11.14})$$

Figure B-11.3 is a plot of the local tangential stress failure obtained from Equation (B-11.14) and the data reviewed in Section 11.2. Approximate heating rates during burst are indicated to

^a Local ballooning will cause the actual value of r_{θ} to be less than the value predicted with Equation (B-11.18).

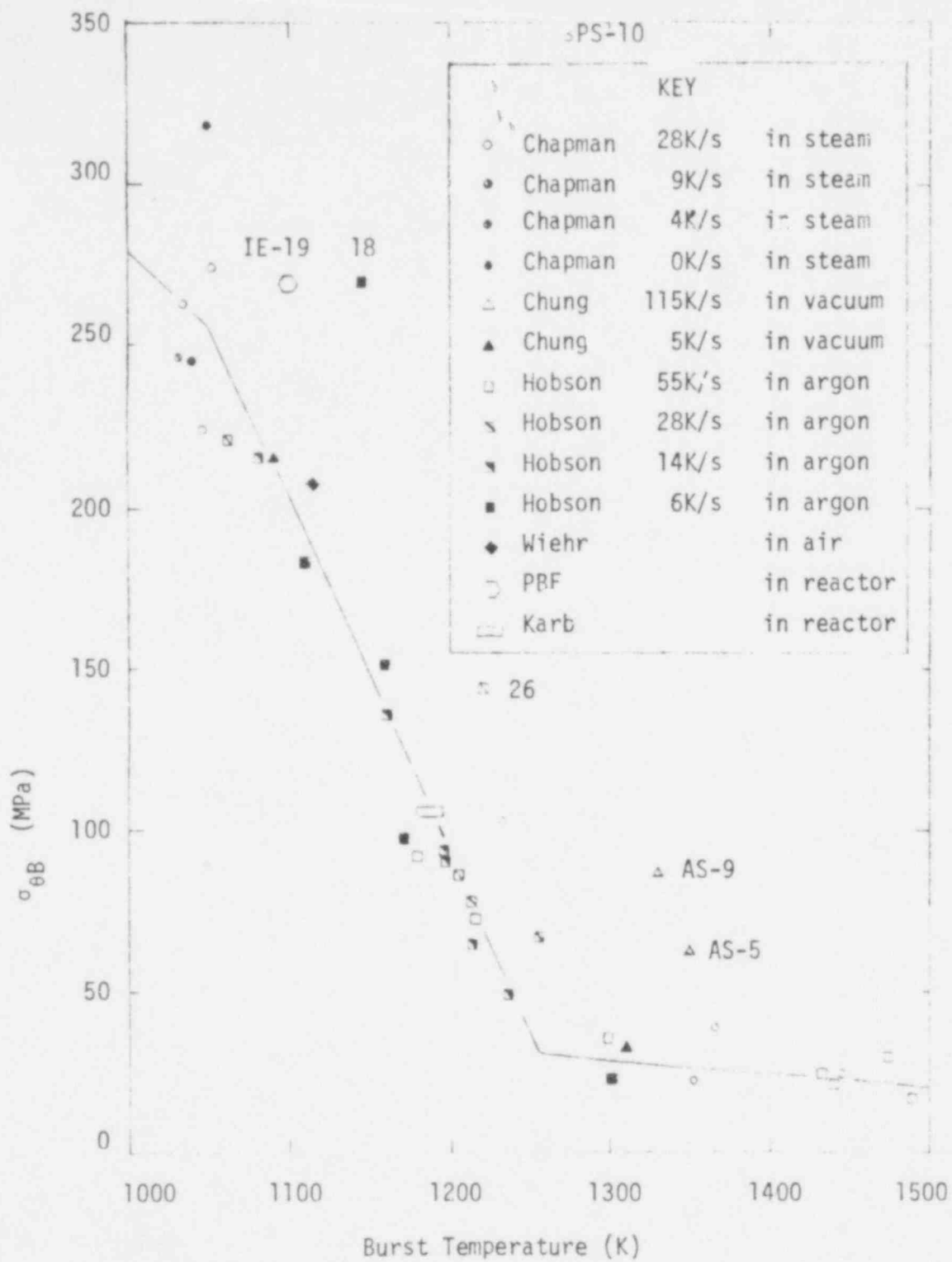


Fig. B-11.2 Local tangential stress at failure versus temperature.

514 272

show that there is no systematic variation with heating rate. Comparison of the burst stresses obtained from Hobson's tests with both Chapman's tests and the two in-reactor data show there is no significant effect of oxide films or alpha layers on the burst stress, at least at heating rates used in these tests. The most probable interpretation of this observation is the suggestion that the relatively thin oxide and alpha layers are cracked before the burst stress of the underlying beta layers is achieved.

Most of the burst stresses shown in Figure B-11.3 are located near a curve which looks very similar to the plot of the strength coefficient for plastic deformation which was obtained in Section B-8.3.2 of this appendix^a. The exceptions are not scattered randomly about the curve. They all lie above the curve. Upon closer inspection, it was noticed that the tests which yielded unusually high tangential burst stresses had some feature which caused one of the assumptions used in calculating tangential burst stress to be questionable. These features are discussed, test by test, in the next several paragraphs.

In the PBF test IE-19 the maximum temperature of the cladding burst region was determined by metallography to be approximately 1100K. Postirradiation examination results^{B-11.15} show the maximum temperature of the fracture area was less than the maximum cladding temperature at other azimuthal locations in the axial plane of the fracture. The interpretation given to this information in the post irradiation examination results report is that 1100K was also the burst temperature because no increase could have occurred on the protruding fracture tips. It is this author's opinion that this conclusion is slightly overstated. The Test Results report (Figure 13 of Reference B-11.19) shows that the adjacent 45° thermocouple which also protruded experienced a 50K temperature rise after the initial

a Figure B-8.5 of interim report CDAP-TR-78-048.

increase. It is therefore probably more realistic to estimate the burst temperature of the cladding in test IE-19 at 1000-1050K.

Test PS-10 from Chapman's studies was performed with a heater which had an unusually large circumferential variation in temperature^{B-11.20}. In this case very local ballooning is likely and Equation (B-11.13) is probably a very poor approximation for the circumferential radius of curvature near burst. Because of the questionable validity of Equation (B-11.13) for this test and because of the large difference between the calculated burst stress of this test and several other data obtained at similar burst temperatures, this test was omitted from the CMLIMi failure analysis.

Test 18 from the Hobson-Rittenhouse series burst at a thermocouple temperature of 1145K (1692^oF) yet had an average circumferential strain characteristic of temperatures in the alpha phase. Moreover, the axial profile of this test is almost triangular (Figure 4 of Reference B-11.9). In all probability the axial radius of curvature in Table B-11.II (estimated from the bottom half of the sample) is much too large. The test was therefore eliminated from the CULIMT data base.

Test 26 from the Hobson-Rittenhouse series is the only sample in the entire test series which did not exhibit approximate mirror symmetry of wall thickness about a plane through the burst area and the cladding center line. In this test one half of the cross section is essentially undeformed and one half is uniformly thin. Thus both the axial and circumferential radii of curvature estimated for this test are questionable and the test was removed from the CMLIMT data base.

Tests AS-9 and AC-5 by Chung are the most difficult of all the data shown in Figure B-11.3 to understand. It is at first tempting to assume that the constraining mandral used in these tests caused a large axial stress which somehow perturbed the test. However, the argument

given in conjunction with Equation (B-11.14) shows that the local axial stress near the failure area was between the yield and the burst stress. Moreover, test AS-36 which differed only in heating rate from AS-5 and AS-9 does not differ from the Hobson or Chapman tests which burst at similar temperatures. Tests AS-5 and AS-9 were tentatively removed from the CMLIMT data base solely because they differ markedly from the two tests by Chapman which were conducted in steam with an internal heater -- two features which are believed to make Chapman's tests more representative of in-reactor cladding failure. However, further analysis of AS-5, AS-9 and corresponding tests by Chung without constraint and/or in steam is recommended to try to understand why the apparent tangential burst stress of AS-5 and AS-9 is so high.

The remaining data shown in Figure B-11.3 and reviewed in Section 11.2 were used to find an expression for the tangential burst stress at failure above 1000 K. Since the failure criterion is intended for use in predicting the final shape of the cladding as well as predicting the time of failure, the failure stress was divided by the strength coefficient used with Equation (B-11.13) and the quotients were averaged. For the alpha phase data with burst temperatures above 1000K the average quotient is 7.48 ± 0.91 , for the alpha + beta region it is 7.54 ± 1.03 and for the beta phase it is 8.14 ± 1.84 . Since there is no significant variation of the quotient, the average obtained for the entire temperature range above 1000 K, 7.70 ± 1.29 , was used to produce Equations (B-11.5C) and (B-11.6).

Equations (B-11.13) and (B-11.14)^a were also used with the low temperature data of Table B-11.IV in an attempt to find low temperature failure stresses. In this case the ratios of failure stress to strength coefficient obtained were much smaller than those of the high

a The axial radius of curvature was assumed to be three times the circumferential radii of annealed cladding and infinite for the irradiated cladding.

temperature data -- 0.84 ± 0.03 for the annealed cladding and 0.80 ± 0.06 for the irradiated cladding. These ratios were not used for the CMLIMT failure stress correlation because the axial radii of curvature used to calculate them were assumed. Instead, the measured failure strains were used with Equation (B-11.8), an assumed strain rate sensitivity exponent of zero and typical anisotropy coefficients^a to calculate failure stresses consistent with Equation (B-11.8) and the measured strain. The approximation is more reasonable than guessing axial radii of curvature at low temperature because (a) the unknown strain rate at failure is unimportant at low temperature and (b) the stress-strain curve at low temperature is very flat -- small uncertainties in stress are equivalent to large uncertainties in strain. The factor of 1.36 for annealed cladding and the recommended increase of burst strength equal to four tenths of the increase in the strength coefficient due to cold work or irradiation in Equation (B-11.5a) reproduce the failure strains listed in Table B-11.IV. Equation (B-11.5b) is simply an assumption contrived to extrapolate between the two regions where data are available without producing unreasonable predictions for failure strain in the temperature range where it is used.

11.4 Application of the Failure Criterion to Determine Cladding Shape after Burst

Equations (B-11.5) are sufficient to provide a complete description of both the time of cladding failure and the shape of failed cladding if they are used with an equation of state for plastic deformation and a mechanical code which models circumferential and axial variations in strain as a function of applied stress and time. Expressions for a

a The irradiated cladding was assumed to be isotropic when effective stress and strains were calculated but the annealed cladding was assumed to have the typical anisotropy coefficients given on page 7 of interim report CDAP-TR-78-048.

mechanical code which has this capability have been found in the literature^{B-11.8}, adapted to treat anisotropic material and modified to work with an equation of state of the form of Equation (B-11.8). These expressions are not presented here because they have not yet been coded and tested against the collection of cladding cross sections and axial profiles that were used to produce the data reviewed in Section 11.2. The expressions derived in this section are intended as consistent alternatives to the direct use of Equation (B-11.5). They also illustrate the effect of deformation history on cladding shape after burst.

The first alternate expression is intended for use with codes like the FRAP-T4 ballooning subcode^{B-11.18} which treat asymmetric deformation but do not calculate local stress. The recommended test for failure is a comparison of wall thickness to the minimum wall thickness given by the following approximate expressions for the strain at failure in an azimuthally symmetric test.

$$\epsilon_r \approx -\epsilon_{\theta SYM} \quad (B-11.15a)$$

$$\text{and } \epsilon_{\theta SYM} = \ln \left[\frac{\sigma_{ZB} t_0}{2 p_B r_Z} + \sqrt{\frac{t_0 \sigma_{\theta B}}{p_B r_0}} + \frac{1}{2} \left(\frac{\sigma_{ZB} t_0}{p_B r_Z} \right) \right] \quad (B-11.15b)$$

where

ϵ_r = local true radial strain at failure (m/m)

$\epsilon_{\theta SYM}$ = true tangential strain at failure for azimuthally symmetric deformation (m/m)

$\sigma_{\theta B}$ = tangential component of true stress at burst (Pa) given by Equations (B-11.5)

- P_B = pressure differential across cladding at burst (Pa)
 r_0 = initial cladding radius (m)
 t_0 = initial cladding wall thickness (m)
 σ_{zB} = axial component of true stress at burst (Pa)
 r_z = axial radius of curvature at burst (m).

If ballooning is neglected ($r_z = \infty$), Equation (B-11.7b) reduces to

$$\sigma_{\theta \text{ SYM}} = \ln \sqrt{\frac{\sigma_{\theta B}}{S_{\theta B}}} \quad (\text{B-11.15c})$$

where

$S_{\theta B}$ = tangential component of engineering stress at burst (Pa)

An outline of the derivation of Equation (B-11.15) follows:

- (1) Following Reference B-11.21, the cladding deformation is considered to be composed of the strain for cylindrical deformation plus a perturbation due to ballooning. Axial strains for isotropic closed tube cylindrical deformation are zero and it is shown in Reference B-11.21 (Equation 4-36) that the change in axial strain due to a balloon with negligible tangential displacement is also zero. It is therefore reasonable to assume that the axial strain for typical bursts is small compared to the radial and tangential strains.
- (2) From the incompressibility relation (true strains sum to zero) and step (1), the true radial strain is minus the true tangential strain in an azimuthally symmetric burst test.

- (3) For an azimuthally symmetric burst test the circumferential radius of curvature and the cladding thickness at burst are related to their initial values by the tangential strain

$$r_{\theta} = r_0 \exp(\epsilon_{\theta \text{sym}}) \quad (\text{B-11.16a})$$

$$t_B = t_0 \exp(-\epsilon_{\theta \text{sym}}) \quad (\text{B-11.16b})$$

- (4) Substitution of Equations (B-11.16) into Equation (B-11.12) and a Taylor series expansion for $\frac{\sigma_{ZB}}{r_Z} \ll \frac{\sigma_{\theta B}}{r_{\theta}}$ yields Equation (B-11.15b) for $\epsilon_{\theta \text{sym}}$.
- (5) If the burst test does not have azimuthal symmetry, Equation (B-11.16a) will overpredict the circumferential radius of curvature^{B-11.18} and Equation (B-16b) will overpredict the cladding wall thickness at failure. However, this is not a serious fault because the local deformation near failure is very rapid. The average strains and thus the average elongation will be only very slightly underpredicted by using Equations (B-11.16b) and (B-11.15b) to predict strain at failure.

The second alternate expressions for determining cladding shape after failure are intended for codes that assume azimuthally symmetric cladding plastic deformation in spite of known temperature differences during the burst. An approximate expression for the effect of temperature variation on circumferential elongation was obtained by correlating to data taken at temperatures near 1050 K^{B-11.10, B-11.22} (Figure 121 in the first reference). The data and least-squares correlation used to describe them are shown in Figure B-11.4. The

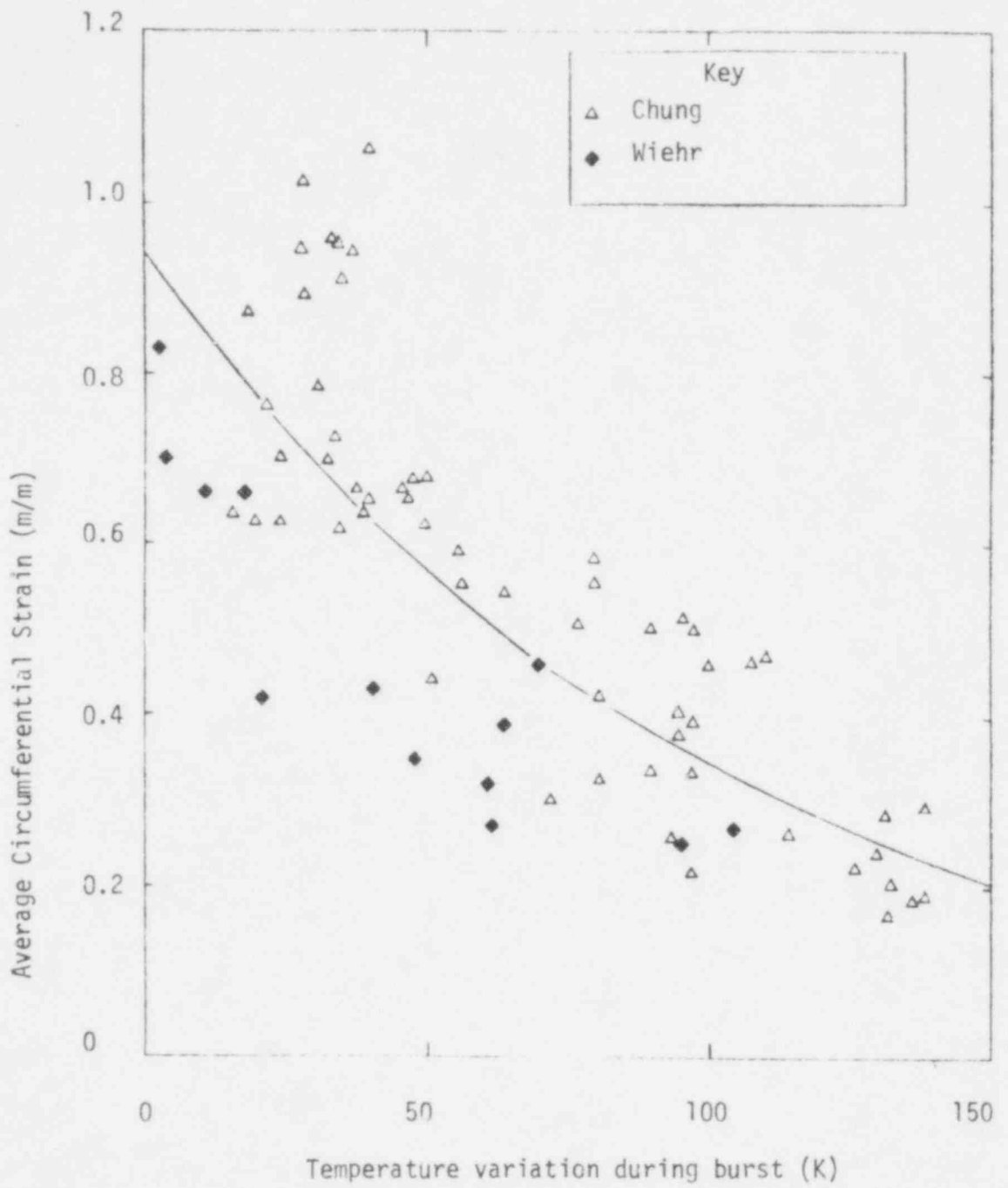


Fig. B-11.4 Base data and MATPRO correlation for effect of temperature variation on average circumferential elongation.

least-squares expression obtained by fitting an exponential function to the data is

$$\bar{e}_\theta = 0.94 \exp (-0.01 \Delta T) \quad (\text{B-11.17})$$

where $\bar{e}_\theta = \frac{(\text{circumference at burst} - \text{initial circumference})}{\text{initial circumference}}$

$\Delta T =$ approximate temperature variation during burst (K)

If the 0.94 of Equation (B-11.17) is replaced by the more general expression of Equation (B-11.15c), the resultant expression for the average circumferential elongation in a typical burst test near 1050 K is:

$$\bar{e}_\theta = \left(\sqrt{\frac{t_o B}{p_B r_o}} - 1 \right) \exp (-0.01 \Delta T) \quad (\text{B-11.18})$$

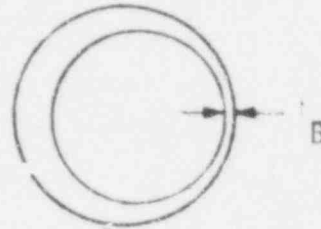
where

$$\bar{e}_\theta = \frac{(\text{circumference at burst} - \text{initial circumference})}{\text{initial circumference}}$$

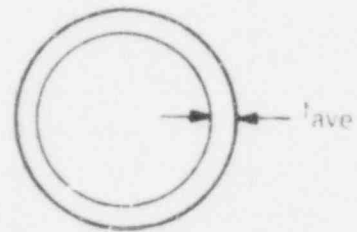
$\Delta T =$ estimated temperature variation around the circumference during burst (K) and the other symbols have been defined previously.

A mechanical model which assumes azimuthal symmetry cannot calculate both the correct average circumference and the correct maximum stress of asymmetric deformation. However, it is possible to define an effective stress which is consistent with Equations (B-11.18) and (B-11.5). This effective burst stress is derived by considering the three cross sections shown in Figure B-11.5.

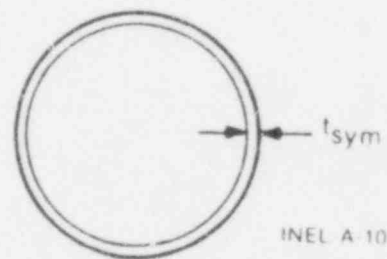
A Asymmetric deformation



B Idealized deformation



C Symmetric deformation



INEL A-10 687

Fig. B-11.5 Schematic cross sections of cladding at burst.

Figure B-11.5A represents the actual asymmetric cladding with local thinning at the hot spot and relatively little deformation at the coolest temperature. Figure B-11.5B represents an idealized symmetric deformation modeled by analytical codes which do not consider asymmetric deformation. The circumference of Figures B-11.5A and B-11.5B are equal. Figure B-11.5C represents a symmetrically deformed cladding with true stress equal to the maximum hoop stress of the actual asymmetric cladding.

The maximum tangential component of true stress of the asymmetric deformation is approximately

$$\sigma_{\theta B} = \frac{P_B r_a}{t_B} \quad (B-11.19)$$

where

r_a = radius of the cladding (m)

and other symbols have been defined previously. The circumferential stress which will be used to predict the idealized deformation is

$$\sigma_{\theta B} = \frac{P_B r_a}{t_{ave}} \quad (B-11.20)$$

where

t_{ave} = wall thickness of the cladding predicted with idealized symmetric deformation (m)

From Equations (B-11.19) and (B-11.20), the tangential stress at failure calculated with idealized deformation is related to the true burst stress by the equation

$$\frac{\sigma_{\theta B}}{\sigma_{\theta B}} = \sigma_{\theta B} \frac{t_B}{t_{ave}} \quad (B-11.21)$$

The ratio $\frac{t_{min}}{t_{ave}}$ in Equation (B-11.21) is related to the reduction in circumferential elongation at failure. Since the maximum true local stress of asymmetric deformation and the circumferential stress of symmetric deformation are both equal to the burst stress,

$$\frac{P_B r_a}{t_B} = \frac{P_B r_{sym}}{t_{sym}} \quad (B-11.22)$$

where

r_{sym} = radius of symmetrically deformed cladding (m)

t_{sym} = wall thickness of symmetrically deformed cladding (m)

and the other terms were defined previously.

The incompressibility relations with the simplifying assumption that axial strain is less than radial or circumferential strain imply that the areas of the idealized and symmetrically deformed cladding are equal. This in turn implies

$$r_a t_{ave} = r_{sym} t_{sym} \quad (B-11.23)$$

Equations (B-11.22) and (B-11.23) can be combined to show

$$\frac{t_B}{t_{ave}} = \left[\frac{r_a}{r_{sym}} \right]^2 \quad (B-11.24)$$

The radii r_a and r_{sym} are related to the circumferential elongation of A and C, (Figure B-11.5)

$$r_a = r_o (1.0 + \bar{e}_\theta) \quad (B-11.25a)$$

$$r_{sym} = r_o (1.0 + e_{\theta_{sym}}) \quad (B-11.26b)$$

$$= r_o \exp(\epsilon_{\theta_{sym}})$$

where

r_o = initial radius of the cladding.

Substitution of Equation (B-11.15C) into Equation (B-11.26), Equations (B-11.25) and (B-11.26) into Equation (B-11.24) and the resultant expression into Equation (B-11.21) yields the following result for effective burst stress

$$\bar{\sigma}_{\theta B} = S_{\theta B} \left[1 + \bar{e}_\theta \right]^2 \quad (B-11.27)$$

where

$\bar{\sigma}_{\theta B}$ = effective burst stress to be used when azimuthally symmetric deformation is assume in spite of known circumferential temperature differences and the other symbols have been defined previously.

The instability strain returned by CMLIMT is also determined with the correlation for typical strain distribution. The expression used in the CMLIMT subcode for instability strain is

$$e_{eI} = \max \left\{ \sqrt[0.05]{\frac{1.15 K t_0}{10^{2m_p} r_0}} - 1 \right\} \exp \left(\frac{-\Delta T}{100} \right) \quad (B-11.28)$$

$$\overline{e}_{eI} = \frac{\text{circumference at instability} - \text{initial circumference}}{\text{initial circumference}}$$

P = pressure differential across cladding (Pa)

K = strength coefficient (Pa)

Equation (B-11.28) was derived by setting the true strain rate in Equation (B-11.8) equal to $10^{-1}/s$ and employing the following simplifying assumptions:

- (1) isotropic texture coefficients and closed tube stress ratios were assumed ($\sigma = 0.866 \sigma_\theta$ and $\epsilon = \epsilon_\theta / 0.866$)
- (2) $\sigma_\theta = S_\theta \exp(2 \epsilon_\theta)$
- (3) Equation (B-11.17) relates average strain to symmetric strain at instability as well as at burst.

One other quantity is calculated and returned by the CMLIMT code. It is intended for users who choose to ignore all the details of the deformation history of the cladding. The quantity returned is a typical engineering burst stress obtained by correlating tests without regard for either the distribution of strain during the tests or the

variation of pressure and temperature with time during the test. If the user is willing to accept the uncertainty associated with using typical burst stresses (pressure) for a given temperature, he can use this relation with all of the previous relations to determine typical average circumferential elongations as a function of burst temperature and the circumferential temperature variation during burst. The correlation used for typical engineering burst stresses is

$$\log_{10} (S) = 8.42 + T [2.78 \times 10^{-3} + T(-4.87 \times 10^{-6} + T 1.49 \times 10^{-9})] \quad (B-11.29)$$

where

S = typical engineering hoop stress at burst (Pa)

T = temperature at rupture (K).

Equation (B-11.29) was obtained by correlating engineering burst stress to burst temperature using data obtained from several sources^{B-11.9, B-11.23 to B-11.29}. Since all information about the local stress and strain has been ignored in producing this correlation, it provides only a typical engineering burst stress as a function of temperature.

Figure B-11.6 shows typical average tangential strains as a function of temperature obtained by substituting typical engineering burst stresses from Equation (B-11.29), true stress at burst from Equation (B-11.5) and several assumed temperature variations during burst into Equation (B-11.18).

11.5 Cladding Mechanical Limits Subcode CMLIMT Listing

The FORTRAN listing of the subcode CMLIMT is given in Table B-11.V.

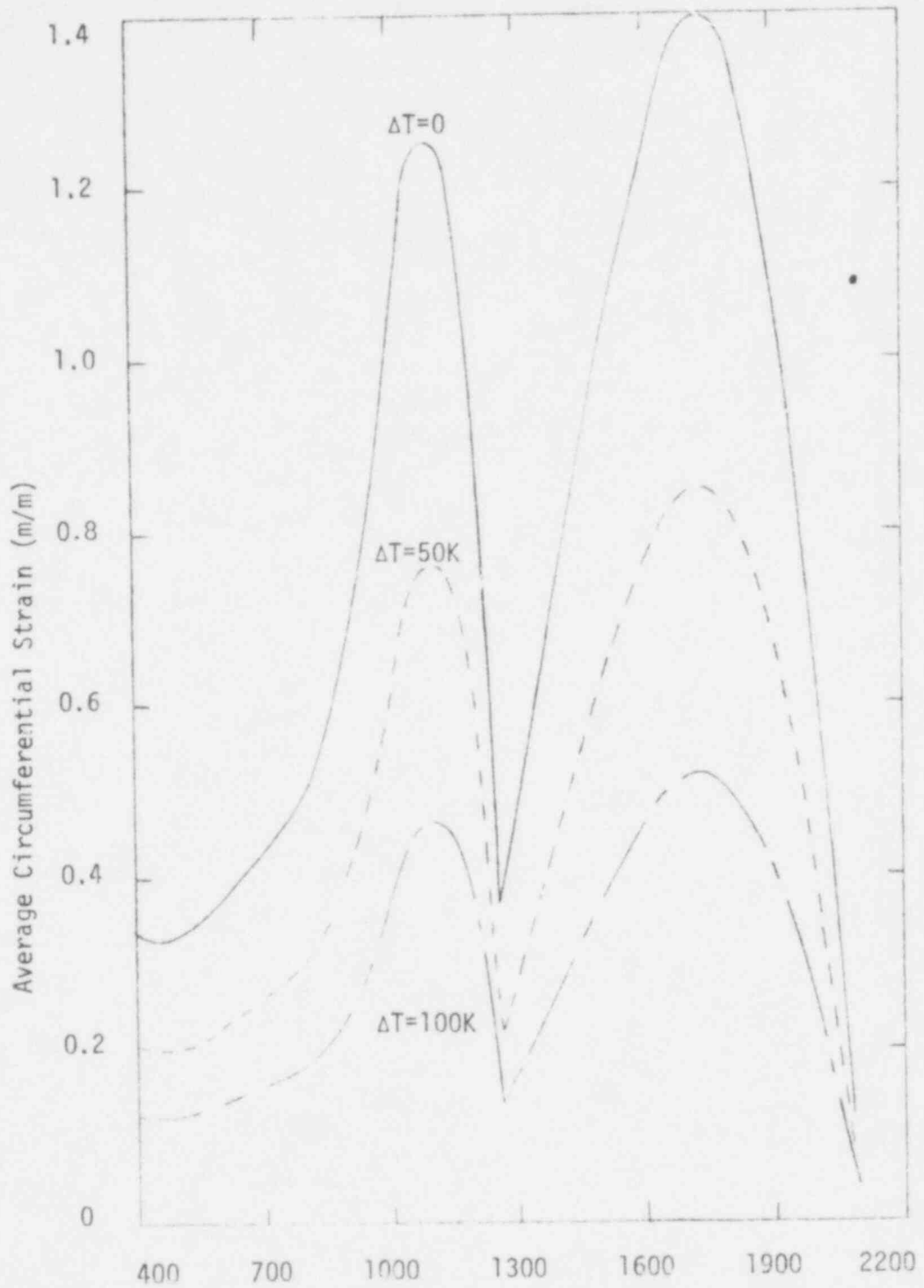


Fig. B-11.6 Typical average circumferential strains predicted by the MATPRO correlations for typical engineering burst stress, true burst stress and typical strain distributions.

TABLE B.II.V (Contd.)

Listing of the CMLIMT Code

CINWID = INPUT INITIAL CLADDING WALL THICKNESS (M)
 CINRAD = INPUT INITIAL CLADDING MIDWALL RADIUS (M)
 CDPRES = INPUT PRESSURE DIFFERENTIAL ACROSS CLADDING AT
 BURST (PA)
 CAXRAD = INPUT AXIAL RADIUS OF CURVATURE (M)
 CAXSTR = INPUT TRUE AXIAL STRESS (M). SET EQUAL TO ZERO
 IN THE SUBCODE IF CAXRAD IS GREATER THAN 10 METERS
 RSTRAN = INPUT STRAIN RATE. (1./S)
 DELTMP = INPUT CIRCUMFERENTIAL TEMPERATURE VARIATION.
 USED ONLY TO FIND TYPICAL VALUES (K)

ESTIMATED VALUES OF DELTMP ARE
 (A) FOR CLADDING WITH EXTERNAL THERMOCOUPLES AND IN FILM
 BOILING DELTMP = 150K
 (B) FOR CLADDING WITH INTERNAL HEATING IN STEAM AND
 WITHOUT EXTERNAL THERMOCOUPLES
 DELTMP = 10 IF THE TEMPERATURE IS ABOVE 1255
 = $50 + (1255 - \text{TEMPERATURE}) / 165 + 10$ IF
 TEMPERATURE IS BETWEEN 1090 AND 1255K
 = 50 IF TEMPERATURE IS BELOW 1090K
 (C) FOR CLADDING IN A FURNACE
 DELTMP = 10
 (D) FOR SELF-RESISTANCE HEATED CLADDING WITH COOL FILLER
 DELTMP = (HEATING RATE)/1000K/S + VALUES OF (B)

THE SUBCODES USED IN THIS SUBROUTINE ARE CKMN AND CELPCD.

THE EQUATIONS USED IN THIS SUBROUTINE ARE BASED ON DATA FROM
 (1) R. H. CHAPMAN, MULTIROD BURST TEST PROGRAM QUARTERLY
 REPORT FOR APRIL - JUNE 1977, ORNL/NUREG/TM-135 (1977).
 (2) R. H. CHAPMAN, J. L. CROWLEY, A. W. LONGEST AND E. G.
 SEWELL, EFFECT OF CREEP TIME AND HEATING RATE ON
 DEFORMATION OF ZIRCALOY-4 TUBES TESTED IN STEAM WITH
 INTERNAL HEATERS, ORNL/NUREG/TM-245 AND NUREG/CR-0345
 (1978).
 (3) R. H. CHAPMAN, MULTIROD BURST TEST PROGRAM QUARTERLY
 PROGRESS REPORT FOR APRIL - JUNE 1976,
 ORNL/NUREG/TM-74, (1977)
 (4) R. H. CHAPMAN, MULTIROD BURST TEST PROGRAM PROGRESS
 REPORT FOR JULY - DECEMBER 1977, ORNL/NUREG/TM-200 AND
 NUREG/CR-0103 (1978).
 (5) R. H. CHAPMAN, MULTIROD BURST TEST PROGRAM PROGRESS
 REPORT FOR JANUARY - MARCH 1978, ORNL/NUREG/TM-217 AND
 NUREG/CR-0225 (1978).
 (6) R. H. CHAPMAN, MULTIROD BURST TEST PROGRAM QUARTERLY
 PROGRESS REPORT FOR JANUARY - MARCH 1976,
 ORNL/NUREG/TM-36 (1976).
 (7) R. H. CHAPMAN, MULTIROD BURST TEST PROGRAM QUARTERLY
 PROGRESS REPORT FOR OCTOBER - DECEMBER 1976,
 ORNL/NUREG/TM-95 (1977).
 (8) R. H. CHAPMAN, MULTIROD BURST TEST PROGRAM QUARTERLY
 PROGRESS REPORT FOR JANUARY - MARCH 1977.

TABLE B.II.V (Contd.)

Listing of the CMLIMIT Code

```

IF(T .LT. 1050.) RATIO = 46.861429* EXP(-(1.9901087E+06/(T**2)))
IF(T .LE. 750.) RATIO = 1.36
IF(T .GE. 1050.) RATIO = 7.7
C FIND ANNEALED STATE STRENGTH COEFFICIENT
AKA = (AK/(1. + ((1120.-(990./ ( EXP((T-1301.5)/61.) + 1.)))
# * DELOXY) - (5.54E-18)*FNCK)/(1. + 0.546*CHKF)
CTSTRT = RATIO * AKA + 0.4 * (5.54E-18 * FNCK + 0.546 * CHKF
# * AKA )
C FIND UNCERTAINTY ESTIMATE FOR CTSTRT
UCTSTT = 0.17 * CTSTRT
C
C FIND TRUE TANGENTIAL FAILURE STRAIN FOR AZIMUTHALLY SYMMETRIC
DEFORMATION
IF(CAXRAD .LT. 1.0E-03) CAXRAD = 1.0E-03
IF(CAXRAD .GT. 1.0E+01) CAXSTR = 0.0
AXFAC = CAXSTR*CINWID/(2.0 * CDPRES*CAXRAD)
STSRPT = ALOG((CTSTRT*CINWID/(CDPRES*CINRAD)))**0.5 + AXFAC *
# (1.0 + 0.5 * AXFAC))
C FIND TYPICAL CIRCUMFERENTIAL ENGINEERING STRAIN AT RUPTURE
STRRPE = ((CTSTRT*CINWID/(CDPRES*CINRAD)))**0.5 - 1.0) *
# EXP(-0.01 * DELTMP)
C
C FIND EFFECTIVE TRUE TANGENTIAL STRESS AT BURST FOR IDEALIZED
SYMMETRIC DEFORMATION AND TYPICAL CIRCUMFERENTIAL STRAIN
CBRSST = (CDPRES * CINPAD / CINRAD ) * ((1.0 + STRRPE)**2.0)
C
C FIND TYPICAL CIRCUMFERENTIAL ENGINEERING STRAIN AT INSTABILITY
STRNIE = (1.0 * CINWID * (10.**((2.*AM))) / (CDPRES * CINRAD
# * (0.866**((1. + AM + AN))))**0.5 - 1.0 )
IF(STRNIE .LT. 0.05) STRNIE = 0.05
STRNIE = STRNIE * EXP(-0.01 * DELTMP)
C
C FIND TYPICAL ENGINEERING HOOP STRESS AT BURST
FT = (CTEMP - 273.15) * 1.8 + 32.
CBRSTE = (10**((5.0E+00*FT*(3.27E-04-FT*(1.14E-06-FT*2.56E-10)))))/
# 1.4505E-04
RETURN
END

```

11.6 References

- B-11.1 R. H. Chapman, Multirod Burst Test Program Quarterly Report for April - June 1977, ORNL/NUREG/TM-135 (December 1977).
- B-11.2 R. H. Chapman, J. L. Crowley, A. W. Longest and E. G. Sewell, Effect of Creep Time and Heating Rate on Deformation of Zircaloy-4 Tubes Tested In Steam with Internal Heaters, ORNL/NUREGITM-245 and NUREG/CR-0345 (October 1978).
- B-11.3 R. H. Chapman, Multirod Burst Test Program Quarterly Progress Report for April - June 1976, ORNL/NUREGITM-74 (January 1977).
- B-11.4 R. H. Chapman, Multirod Burst Test Program Progress Report for July - December 1977, ORNL/NUREGITM-200 and NUREG/CR-0103 (June 1978).
- B-11.5 R. H. Chapman, Multirod Burst Test Program Progress Report for January - March 1978, ORNL/NUREG/TM-217 and NUREG/CR-0225 (August 1978).
- B-11.6 R. H. Chapman, Multirod Burst Test Program Quarterly Progress Report for January - March 1976, ORNL/NUREG/TM-36 (September 1976).
- B-11.7 R. H. Chapman, Multirod Burst Test Program Quarterly Progress Report for October - December 1976, ORNL/NUREG/TM-95 (April 1977).
- B-11.8 R. H. Chapman, Multirod Burst Test Program Quarterly Progress Report for January - March 1977, ORNL/NUREG/TM-108 (May 1977).

- B-11.9 D. O. Hobson and P. L. Rittenhouse, Deformation and Rupture Behavior Behavior of Light-Water Reactor Fuel Cladding, ORNL-4727 (October 1971).
- B-11.10 H. M. Chung and T. F. Kassner, Deformation Characteristics of Zircaloy Cladding in Vacuum and Steam Under Transient-heating Conditions: Summary Report, ANL-77-31 and NUREG/CR-0344 (July 1978).
- B-11.11 A. A. Bauer, L. M. Lowry and J. S. Perrin, Evaluating Strength and Ductility of Irradiated Zircaloy. Quarterly Progress Report January through March, 1976, BMI-NUREG-1948 (March 1976).
- B-11.12 A. A. Bauer, W. J. Gallagher, L. M. Lowry and A. J. Markworth, Evaluating Strength and Ductility of Irradiated Zircaloy. Quarterly Progress Report July through September, 1977, BMI-NUREG-1985 (October 1977).
- B-11.13 A. A. Bauer, W. J. Gallagher, L. M. Lowry and A. J. Markworth, Evaluating Strength and Ductility of Irradiated Zircaloy. Quarterly Progress Report October through December, 1977, BMI-1992 and NUREG/CR-0026 (January, 1978).
- B-11.14 D. W. Croucher, Behavior of Defective PWR Fuel Rods During Power Ramp and Film Boiling Operation, TREE-1267 and NUREG/CR-0283 (February 1979).
- B-11.15 T. F. Cook, S. A. Ploger and R. R. Hobbins, Postirradiation Examination Results for the Irradiation Effects test IE-5, TREE-NUREG-1201 (March 1978).

- B-11.16 E. H. Karb, "Results of the FR-2 Nuclear Tests on the Behavior of Zircaloy Clad Fuel Rods," paper presented at the 6th NRC Water Reactor Safety Research Information Meeting, Gaithersburg, MD, November 7, 1978.
- B-11.17 K. Wiehr, He Schmidt, Out-of-Pile Versuche zume Aufblahvorgang von Zirkaloy-Hüllen. Ergebnisse aus Vorversuchen mit verkürzter Brennstabsimulatoren, KfK 2345 (October 1977).
- B-11.18 L. J. Siefken, M. P. Bohn, S. O. Peck, J. A. Dearien, E. T. Laats, FRAP-T5 A Computer Code for the Transient Analysis of Oxide Fuel Rods, CDAP-TR-79-043 (March 1979) page 114.
- B-11.19 D. W. Croucher, T. R. Yackle, C. M. Allison and S. A. Ploger, Irradiation Effects Test Series IE 5 Test Results Reprt, TREE-NUREG-1130 (January 1978).
- B-11.20 R. H. Chapman, Multirod Burst Test Program Quarterly Progress Report for October - December 1975, ORNL/NUREG/TM-10 (May 1976).
- B-11.21 J. M. Kramer and L. W. Deitrich, Cladding Failure by Local Plastic Instability, ANL-77-95 (December 1977).
- B-11.22 K. Wiehr et al, Jahreskolloquim 1977 des Projekts Nukleare Sicherheit.
- B-11.23 C. C. Busby and K. B. Marsh, High Temperature Deformation and Burst Characteristics of Recrystallized Zircaloy-4 Tubing, WAPD-T-900 (January 1970).

- B-11.24 D. G. Hardy, "Burst Testing of Zircaloy Cladding from Irradiated Pickering-type Fuel Bundles," Symposium on the Effects of Radiation on Substructure and Mechanical Properties of Metals and Alloys, Los Angeles, June 25-30, 1972, ASTM-STP 529 (1973) pp 415-435.
- B-11.25 M. F. Osborne and G. W. Parker, The Effect of Irradiation on the Failure of Zircaloy-clad Fuel Rods, ORNL-3626 (January 1972).
- B-11.26 D. O. Hobson, M. F. Osborne, G. W. Parker, "Comparison of Rupture Data from Irradiated Fuel Rods and Unirradiated Cladding," Nuclear Technology, 11 (August 1971).
- B-11.27 D. G. Hardy, "The Effect of Neutron Irradiation on the Mechanical Properties of Zirconium Alloy Fuel Cladding in Uniaxial and Biaxial Tests," Symposium on Irradiation Effects on Structural Alloys for Nuclear Reactor Application, Niagara Falls, Canada, June 29-July 1, 1970, ASTM-STP 484 (1971) pp 215-216.
- B-11.28 W. J. Langford, "Metallurgical Properties of Cold-Worked Zircaloy-2 Pressure Tubes Irradiated Under CANDU-PHW Power Reactor Conditions," Symposium on Irradiation Effects on Structural Alloys for Nuclear Reactor Application, Niagara Falls, Canada, June 29-July 1, 1970, ASTM-STP 484 (1971) pp 259-286.
- B-11.29 W. R. Smalley, Saxton Core II Fuel Performance Evaluation Material, WCAP-3385-56 (September 1971) pp 4-84, 4-65; W. R. Smalley, Evaluation of Saxton Core III Fuel Materials Performance, WCAP-3385-57 (July 1974) pp 3-69, 3-132, 3-134.